Mon. Not. R. Astron. Soc. **000**, 000–000 (2000)

Small-scale inviscid accretion discs around black holes

Andrei M. Beloborodov[1,2] and Andrei F. Illarionov[1,2]
[1] *Stockholm Observatory, SE-133 36 Saltsjöbaden, Sweden*
[2] *Astro-Space Center of Lebedev Physical Institute, Profsoyuznaya 84/32, 117810 Moscow, Russia*

Accepted, Received

ABSTRACT
Gas falling quasi-spherically onto a Schwarzschild black hole can form an inner thin accretion disc if its specific angular momentum, l, exceeds $l_* \approx 0.75 r_g c$, where r_g is the Schwarzschild radius. The standard disc model assumes $l \gg l_*$. We argue that in many black-hole sources the accretion flows can have $l \gtrsim l_*$, and assess the mechanism of accretion in this regime. In a range $l_* < l < l_{\rm cr}$, a small-scale disc forms in which gas overcomes the centrifugal barrier and spirals fast into the black hole without any help of horizontal viscous stresses. Such an "inviscid" disc, however, interacts inelastically with the infall feeding the disc, which leads to energy dissipation. This interaction determines the disc dynamics and luminosity. We find the radiative efficiency of this accretion regime to be comparable with the efficiency of the standard disc. The maximum radius of the fast inviscid disc is $r_{\max} \approx 2l_{\rm cr}^2/r_g c^2 \sim 14 r_g$, and the energy release peaks at about $2r_g$. The disc emits a standard Comptonized X-ray spectrum, a power-law with a break at ~ 100 keV. This regime is likely to take place in wind-fed X-ray binaries and is also possible in active galactic nuclei.

Key words: accretion, accretion discs — binaries: general — black hole physics — radiative mechanisms: thermal — X-rays: galaxies — X-rays: stars

1 INTRODUCTION

Spherical accretion flows onto black holes (BHs) have low radiative efficiencies (Shvartsman 1971; Shapiro 1973; but see also Bisnovatyi-Kogan & Ruzmaikin 1974; Mészáros 1975). If the flow is slightly rotating, the situation can change crucially: a small-scale accretion disc can form around the BH, which has a high efficiency, and then the BH "switches on" as a luminous source. The condition for formation of a thin disc around a Schwarzschild black hole reads $l > l_*$, where l is the specific angular momentum of the accreting matter and $l_* = 0.75 r_g c$ (see Section 2.2), $r_g = 2GM/c^2$ being the Schwarzschild radius. The standard disc model assumes $l \gg l_*$ (see Pringle 1981 for a review). High-l discs can form, e.g., in X-ray binaries fed by streams from Lagrangian L_1 point.

By contrast, in wind-fed X-ray binaries, the accretion flows are quasi-spherical, with $l \sim l_*$, just about critical for the disc formation (see, e.g., Frank, King, & Raine 1985 for a review). The average l of the accreting wind matter is $\bar{l} = \zeta(1/4)\Omega R_a^2$ (Illarionov & Sunyaev 1975; Shapiro & Lightman 1976), where $R_a = 2GM/w^2 \sim 10^{11}$ cm is the accretion radius, $w \approx 10^8$ cm s^{-1} is the wind velocity, Ω is the angular velocity of the binary, and $\zeta \sim 1$ is a numerical factor. Three X-ray binaries have been classified as massive ones with black hole companions: Cyg X-1, LMC X-1, and LMC X-3 (see Tanaka & Lewin 1995). They have orbital periods $P = 2\pi/\Omega = 5.6$, 4.2, and 1.7 d, respectively. Hence, $\bar{l} \approx 1.5\zeta P^{-1}(M/{\rm M}_\odot)(w/10^8)^{-4} r_g c \sim r_g c$ in these objects. It implies marginal formation of a small-scale disc. Whether the disc forms or not depends on the precise value of angular momentum which is difficult to calculate because the details of wind accretion are not fully understood (note the strong dependence of $\bar{l}$ on the wind velocity, w). The fact that the objects are luminous indicates that a disc does form.

Small-scale accretion discs may also form around massive black holes in active galactic nuclei (AGNs). There, the source of accreting gas is uncertain. One possibility is gas production by a surrounding star cluster owing to star-star collisions and/or tidal disruption of stars by the BH (Hills 1975). Then quasi-spherical accretion flow can form with a modest angular momentum, comparable to l_*.

The regime $l \gtrsim l_*$ can be widespread among luminous black-hole sources. Note that only a small number of wind-fed BH binaries and galactic nuclei are active, and most of the unseen objects may accrete in the spherical regime with $l < l_*$, with a low luminosity. The observed bright sources with $l > l_*$ are then in the "tail" of the distribution of objects over angular momentum, ${\rm d}N/{\rm d}l$, which falls off towards high l. Then most of the bright sources can have $l \gtrsim l_*$, being just near the threshold for the disc formation.

In this paper, we construct an axisymmetric model of accretion with $l \gtrsim l_*$. The Compton-cooled infalling matter reaches the deep potential well on the free-fall time-scale and liberates energy in inelastic collision with the small-scale disc formed in the symmetry plane of the flow. Accretion then proceeds via thin disc into the BH. The disc interacts with the infalling flow, which allows the spiraling gas to overcome the centrifugal potential barrier without any help of horizontal viscous stresses. Such a disc is drastically different

from its standard counterpart as regards the mechanism of energy release and the emission spectrum.

The paper is organised as follows. In Section 2, we study the axisymmetric free fall in the gravitational field of a Schwarzschild BH and discuss the caustic in the equatorial plane (the collision plate) where the accretion disc is formed. In Section 3, we write down basic equations of the disc and solve the equations numerically. As a result, we get a model for the disc structure and find the efficiency of accretion. Most of the energy is released quite close to the event horizon, at $\sim 2r_g$, and the problem requires exact relativistic treatment. All the calculations are relativistic (assuming a non-rotating BH). For comparison, in Section 4, we also formulate and compute an analogous Newtonian problem. The results and issues for further study are discussed in Section 5.

2 FORMATION OF A SMALL-SCALE DISC

Consider an axisymmetric accretion flow which is slowly rotating around the polar axis, so that the non-radial velocity $v_\perp \approx v_\varphi \ll v_r$ at $R \gg r_g$. At large distances, the flow is almost spherical. As a result of Compton cooling by the inner source, the flow becomes super-sonic inside the Compton radius, $R_{\rm C} \sim 10^4 r_g$ (see, e.g., Illarionov & Kompaneets 1990). At $R < R_{\rm C}$, the matter accretes along ballistic parabolic trajectories which we study in this section. The freely falling flow in Newtonian gravity is discussed in detail in Illarionov & Beloborodov (2000, hereafter IB2000). Here, we need the relativistic equations since the typical radius at which accretion switches from the spherical to a disc-like regime, $R_d \sim l^2/r_g c^2$, is comparable to r_g in our problem. Hereafter label "∞" corresponds to distances $R \gg R_d$ (but $R < R_{\rm C}$).

2.1 Free fall

Let λ be proper time along a ballistic trajectory in the Schwarzschild space-time. Denote the orbital angular momentum of the trajectory by $\mathbf{l}$. The z-component of the angular momentum is $l_z = l\sin\theta_\infty$ where θ_∞ is the polar angle of the trajectory at $R \gg R_d$. The specific orbital energy for a parabolic trajectory is $E = c^2$. The equations of motion in Schwarzschild (R,θ,φ)-coordinates then read (see, e.g., Misner, Thorne, & Weeler 1973):

$$R^2\frac{{\rm d}R}{{\rm d}\lambda} = -\sqrt{r_g c^2 R^3 - l^2R^2(1-\frac{r_g}{R})}, \tag{1}$$

$$R^2\frac{{\rm d}\theta}{{\rm d}\lambda} = l_z\sqrt{{\rm ctg}^2\theta_\infty - {\rm ctg}^2\theta}, \tag{2}$$

$$R^2\frac{{\rm d}\varphi}{{\rm d}\lambda} = \frac{l_z}{\sin^2\theta}. \tag{3}$$

The only difference from the corresponding Newtonian equations is the presence of the additional factor $(1-r_g/R)$ in equation (1).

One can solve equations (1-3) for the trajectory $\theta(R),\varphi(R)$,

$$\cos\theta = \cos\theta_\infty\cos\psi, \tag{4}$$

$$\sin(\varphi-\varphi_\infty) = \frac{\sin\psi}{\sin\theta}, \tag{5}$$

$$\psi(R) = \int_R^\infty \frac{l\,{\rm d}R}{\sqrt{r_g c^2R^3 - l^2R^2(1-r_g/R)}}. \tag{6}$$

Equations (4,5) are identical to non-relativistic equations (9,10) in IB2000. The relativistic effects alter the expression for ψ only (the additional factor $(1-r_g/R)$ results in the elliptical integral [6]). In the non-relativistic limit, $r_g/R \to 0$, the integral (6) gives the Newtonian expression $\cos\psi = 1 - l^2/GMR$ (see eq. [8] in IB2000).

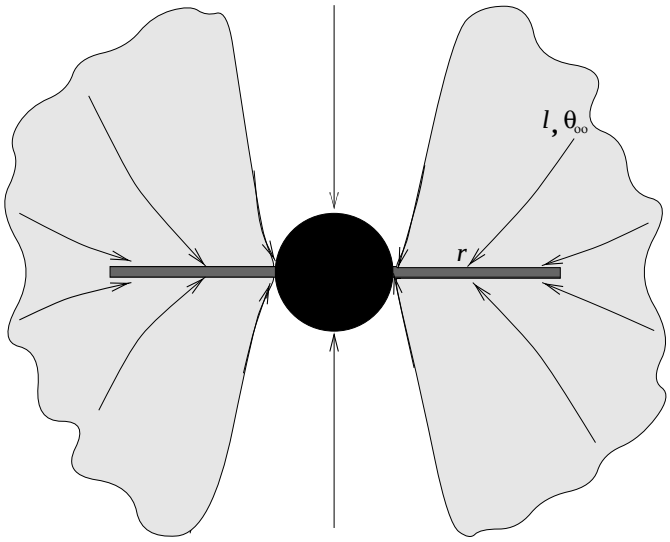

Figure 1. Schematic picture of the disc formation. The inflow through S_∞ has an angular momentum, l, increasing towards the equatorial plane, ${\rm d}l/{\rm d}\sin\theta_\infty > 0$. The collision radius, which is a growing function of l, monotonically increases as θ_∞ approaches $\pi/2$. The shadowed region shows the part of the accretion flow that collides outside r_g and forms a couple of radiative shocks which sandwich the collision plate. The other part of the flow (at small polar angles) is directly swallowed by the black hole with a low radiative efficiency.

The inflow streamlines $\theta(R),\varphi(R)$ induce a mapping of sphere S_∞ onto each sphere S_R of radius R. The mapping $(\theta_\infty,\varphi_\infty) \to (\theta_R,\varphi_R)$ is one-to-one if the Jacobian $\Delta \equiv \partial(\cos\theta_R,\varphi_R)/\partial(\cos\theta_\infty,\varphi_\infty) \neq 0$ for any $\theta_\infty,\varphi_\infty$. The flow is axisymmetric, and hence $\partial\cos\theta_R/\partial\varphi_\infty = 0$ and $\partial\varphi_R/\partial\varphi_\infty = 1$. Taking this into account, one gets the Jacobian,

$$\Delta = \frac{{\rm d}\cos\theta_R}{{\rm d}\cos\theta_\infty} = \cos\psi - \cos\theta_\infty\sin\psi\frac{{\rm d}\psi}{{\rm d}\cos\theta_\infty}.$$

The Jacobian stays positive outside the equatorial plane if $\cos\theta_\infty {\rm d}\psi/{\rm d}\cos\theta_\infty < 0$. Since ψ increases with increasing l, this condition can be rewritten as

$$\frac{{\rm d}l}{{\rm d}\sin\theta_\infty} > 0. \tag{7}$$

This is the condition for the absence of streamline intersections outside the equatorial plane. It is exactly the same as in Newtonian case (see IB2000). For example, condition (7) is satisfied if matter is in solid body rotation at S_∞, $l = l_0\sin\theta_\infty$. Then the ballistic streamlines intersect only when they reach the equatorial plane (see Fig. 1). The loci of intersections form a two-dimensional caustic, the collision plate.

2.2 The collision plate

We use the polar coordinates (r,φ) on the equatorial plane, $\theta = \pi/2$. A streamline coming from $\theta_\infty,\varphi_\infty$ to the collision point (r,φ) executes 1/4 of the full turn around the polar axis, $\varphi =$

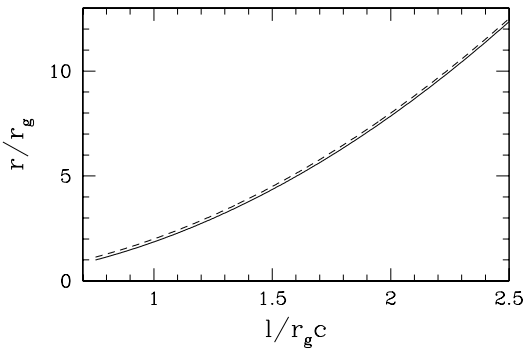

Figure 2. The collision radius $r(l)$. The solid curve shows the result of exact relativistic calculations (see eq. [8]). The dashed curve shows the Newtonian approximation, $r = l^2/GM$.

$\varphi_\infty + \pi/2$, precisely in the same way as it does in Newtonian gravity (see IB2000 and eq. [4,5]).

The radius of collision is affected by the relativistic effects. A streamline reaches the equatorial plane at $\psi = \pi/2$ (see eq. [4]) which, combined with equation (6), gives the exact relativistic equation for the collision radius, r, of two symmetric streamlines with angular momentum l,

$$\int_r^\infty \frac{\mathrm{d}R}{\sqrt{r_g c^2 R^3 - l^2 R^2 (1 - r_g/R)}} = \frac{\pi}{2l}. \tag{8}$$

The equation involves the elliptic integral. At $r \gg r_g$, it is simplified and yields the Newtonian relation, $r = l^2/GM$. Note that the relativistic effects do not crucially alter the Newtonian expression. The maximum deviation of the exact $r(l)$ from l^2/GM is reached at $r = r_g$, and this deviation is within 15 percent (see Fig. 2).

The collision occurs outside the event horizon if angular momentum exceeds a minimum value, l_*, such that $r(l_*) = r_g$. From equation (8) one finds $l_* \approx 0.754 r_g c$. (In the Newtonian approximation, one gets $l_* = r_g c/\sqrt{2} \approx 0.707 r_g c$.) A streamline with $l < l_*$ goes directly into the BH without intersecting other streamlines. A streamline with $0.754 < l/r_g c < 2$ would also end up in the BH if continued on the other side of the equatorial plane (see, e.g., Novikov & Frolov 1989). The collision in the equatorial plane, however, happens before that.

Assuming (7), streamlines starting at $\theta_\infty \to \pi/2$ have the largest angular momentum, $l \to l_0$, and, therefore, they have the largest collision radius, $r_0 \approx l_0^2/GM$. The resulting caustic in the equatorial plane is a plate of radius r_0 (see Fig. 1). The plate forms outside the event horizon if $r_0 > r_g$, or, equivalently, if $l_0 > l_* \approx 0.754 r_g c$. For comparison, the threshold for formation of a standard disc outside $3r_g$ exceeds $\sqrt{3} r_g c$ (see Beloborodov & Illarionov 2000).

The free-fall equations (1-3) give all the parameters of the flow in the preshock region just above/below the collision plate. Note that the azimuthal velocity component is about the radial one.

2.3 The held-down shocks and vertical mixing

The collision of two symmetric super-sonic streams falling onto the equatorial plane results in two collisionless shocks forming on both sides of the plane. The vertical component of the plasma velocity is reduced in the shock by ξ times where $\xi \geq 4$ is the compression in the shock ($\xi = 4$ if most of the heat released goes to the ions). The horizontal velocity remains unchanged. Horizontal motion can stay super-sonic after passing the shock.

The kinetic energy of matter is partly transformed into heat in the shock. Most of the energy is likely to be passed to the ions, though some unknown fraction, ϵ, may go to the electrons (studies of interplanetary and interstellar shocks indicate $\epsilon \sim 0.2 - 0.3$, see Draine & McKee 1993). The electrons immediately radiate the received energy away and then take the energy from the ions. The resulting radiative capability of the shocked plasma depends on ϵ and also on the rate of energy exchange between the protons and the electrons. The minimal e-p coupling is provided by Coulomb collisions. Owing to Coulomb collisions, the electrons of temperature T_e cool the protons of temperature T_p on the time-scale (Spitzer 1962),

$$t_{\mathrm{Coul}} = \frac{\sqrt{\pi/2} m_p \theta_e^{3/2}}{m_e c \sigma_{\mathrm{T}} n \ln\Lambda} \approx 17 \frac{T_e^{3/2}}{n} \mathrm{s}, \tag{9}$$

where n is the plasma density, and a Coulomb logarithm $\ln\Lambda = 15$ and $\theta_e \equiv kT_e/m_e c^2 < 1$ are assumed. The e-p coupling can be enhanced by collective plasma effects, so that the proton cooling time-scale is $t_{\mathrm{ep}} = \chi^{-1} t_{\mathrm{Coul}}$, where $\chi > 1$.

The shock is held-down to the equatorial plane if t_{ep} is shorter than $\xi r/v_{\mathrm{ff}}$, where $v_{\mathrm{ff}} \sim c(r_g/r)^{1/2}$ is the typical upstream (free-fall) velocity. The density in the downstream region can be estimated in terms of the accretion rate, $\dot{M}_{\mathrm{tot}}$: $n \sim \xi \dot{M}_{\mathrm{tot}}/4\pi r^2 m_p v_{\mathrm{ff}}$ (here, we have taken into account the compression in the shock, ξ). One then gets,

$$\frac{v_{\mathrm{ff}} t_{\mathrm{ep}}}{\xi r} \sim \frac{\sqrt{2\pi} m_p \theta_e^{3/2}}{\ln\Lambda\, m_e \xi^2 \chi \dot{m}}, \tag{10}$$

where $\dot{m} = \dot{M}_{\mathrm{tot}} c^2/L_{\mathrm{E}}$ is the dimensionless total accretion rate onto the BH, $L_{\mathrm{E}} = 2\pi r_g m_p c^3/\sigma_{\mathrm{T}}$ is the Eddington luminosity.

The electron temperature in the downstream region can be found from the energy balance,

$$\frac{T_e}{t_{\mathrm{C}}} = \frac{T_p}{t_{\mathrm{ep}}}, \tag{11}$$

where $t_{\mathrm{C}} = 3m_e c/8\sigma_{\mathrm{T}} U$ is the Compton cooling time-scale and U is the radiation energy density. For a radiatively efficient shock, the proton thermal energy is finally radiated, resulting in a radiation flux $F \sim (3/2) nkT_p v_{\mathrm{ff}}/\xi$. It yields an estimate, $U \sim 2F/c \sim 3nkT_p v_{\mathrm{ff}}/c\xi$, and hence

$$t_{\mathrm{C}} = \frac{3m_e c}{8\sigma_{\mathrm{T}} U} \sim \frac{m_e c^2 \xi}{8\sigma_{\mathrm{T}} nkT_p v_{\mathrm{ff}}}.$$

The energy balance (11) then yields

$$\theta_e \sim \left(\frac{\ln\Lambda\, m_e}{\sqrt{2\pi} m_p} \frac{\xi\chi c}{4v_{\mathrm{ff}}} \right)^{2/5} \approx 0.1 \left(\frac{\xi\chi c}{4v_{\mathrm{ff}}} \right)^{2/5}. \tag{12}$$

$v_{\mathrm{ff}} \propto r^{-1/2}$, and hence $\theta_e \propto r^{1/5}$.

The hot downstream layer radiating most of the proton heat has optical depth $\tau_{\mathrm{T}} \sim (v_{\mathrm{ff}}/\xi) t_{\mathrm{ep}} n \sigma_{\mathrm{T}}$. It satisfies the relation, $\tau_{\mathrm{T}} \theta_e \sim 0.1$ (as follows from eqs. [9] and [12]), i.e, $\tau_{\mathrm{T}} \sim 1$ for typical $\theta_e \sim 0.1$. With more exact approach, the unsaturated Comptonization in the hot layer involves radiative transfer with multiple

scatterings, and $\tau_{\rm T} \sim 1$ corresponds to the condition $y \sim 1$ where y is the Kompaneets' parameter (see, e.g., Rybicki & Lightman 1979). In deeper layers, at $\tau_{\rm T} > 1$, the downstream temperature (both T_p and T_e) falls off sharply (see Zel'dovich & Shakura 1969, Shapiro & Salpeter 1975 for a similar shock on the surface of a neutron star).

From equations (10) and (12) one gets,

$$\frac{v_{\rm ff} t_{\rm ep}}{\xi r} \sim \frac{2}{\xi \dot{m}} \left(\frac{4}{\xi\chi}\right)^{2/5} \left(\frac{c}{v_{\rm ff}}\right)^{3/5} \sim \frac{0.05}{\dot{m}\theta_e} \left(\frac{4}{\xi}\right) \left(\frac{c}{v_{\rm ff}}\right). \quad (13)$$

We are interested here in sub-Eddington accretion discs, with luminosities $L < L_{\rm E}$, so that the free-fall approximation can be used above the equatorial plane. It requires $\dot{m} < \dot{m}_{\rm E} = \eta^{-1}$ where η is the radiative efficiency of the disc (see Section 3.7 and Fig. 6). In the range $0.05\theta_e^{-1} \lesssim \dot{m} < \eta^{-1}$ we have sub-Eddington accretion with radiatively efficient shocks held-down to the equatorial plane.

This pattern of accretion is different from previously considered situation with shocks formed far from the equatorial plane (e.g., Igumenshchev, Illarionov, & Abramowicz 1999). The shock would be detached if the plasma had a low radiative capability, so that the pressure builds up behind the shock and drives it away from the plane. In that case, when the shock gets detached so much that it acquires a quasi-spherical shape, it continues unstable expansion to larger radii and stationary accretion becomes impossible (Igumenshchev et al. 1999).

We hereafter assume that the accretion rate is high enough, so that the condition $t_{\rm ep} < \xi r/v_{\rm ff}$ is satisfied and the shocks are held-down. We thus have free-falling gas everywhere above and below the thin disc of shocked plasma. The disc has a finite half-thickness, H, supported by the pressure, $p_d \sim \rho_d c_s^2$, against the ram pressure of the infall, $p_{\rm ff} \sim \rho_{\rm ff} v_{\rm ff}^2$. Here, ρ_d and c_s are the density and the sound speed in the midplane of the disc, and $\rho_{\rm ff}$ is the density of the infall. The pressure balance yields $\rho_d/\rho_{\rm ff} \sim (v_{\rm ff}/c_s)^2$. The regime of held-down shocks implies efficient radiative cooling, and we have $c_s \ll v_{\rm ff}$ and $\rho_d \gg \rho_{\rm ff}$. The accretion velocity in the disc is comparable to $v_{\rm ff}$ (see Section 3), and, from matter conservation, we estimate $H/r \sim \rho_{\rm ff}/\rho_d \sim (c_s/v_{\rm ff})^2$.

At a given radius, the disc is composed of matter that entered the disc at larger radii with different horizontal velocities. A strong turbulence is likely to develop in the disc under such conditions. The turbulence can mix up the disc in the vertical direction on a time-scale $\sim H/c_s$ which is $\sim c_s/v_{\rm ff}$ shorter than the accretion time-scale, $t_a \sim r/v_{\rm ff}$. In the mixing process, the random motions above the level $\sim \rho_d c_s^2$ are converted into heat, and the disc acquires a vertically-averaged horizontal velocity (with both radial and azimuthal components). The released heat is radiated away, contributing to the total luminosity of the disc.

When absorbing the infalling matter, the disc also absorbs horizontal momentum and its velocity changes. The process can be described as inelastic collision which is governed by the corresponding law of momentum conservation (see Section 3). A similar approximation was used in the study of the accretion line in the Bondi-Hoyle-Lyttleton problem (see Bondi & Hoyle 1944). The energy released in the process of the infall-disc interaction determines the radiative efficiency of accretion.

3 FAST INVISCID ACCRETION DISC

The shocked turbulent gas continues to accrete onto the BH through the thin disc in the equatorial plane. We show in this section that if l_0 is smaller than some specific value $l_{\rm cr}$, then accretion in the disc occurs fast: the gas spirals into the BH on the free-fall time-scale. Turbulent diffusion, which efficiently mixes up the disc in the vertical direction (see Section 2.3), has a negligible effect on horizontal motion, and the disc can be assumed to be inviscid. Hereafter in this section, we solve the stationary problem of disc accretion in this regime and compute $l_{\rm cr}$. In numerical calculations we assume solid body rotation of the inflow at S_∞,

$$l(\theta_\infty) = l_0 \sin\theta_\infty. \quad (14)$$

3.1 Accretion rate

The asymptotically spherical inflow at S_∞ has a total accretion rate $\dot{M}_{\rm tot}$ and homogeneous distribution $\mathrm{d}\dot{M}/\mathrm{d}\Omega_\infty = \dot{M}_{\rm tot}/4\pi$ where $\mathrm{d}\Omega_\infty = \mathrm{d}\varphi_\infty \mathrm{d}\cos\theta_\infty$. The distribution of angular momentum, $l(\theta_\infty)$, satisfies condition (7), so that streamlines with $\sin\theta'_\infty > \sin\theta_\infty$ have angular momenta $l'(\theta'_\infty) > l(\theta_\infty)$ and collision radii $r'(l') > r(l)$ (see Fig. 1). All the matter impinging the disc finally accretes onto the BH. Hence, the disc accretion rate at a radius r, $\dot{M}(r)$, equals the rate of matter supply to the disc at $r' > r$, which in turn equals the rate of accretion through the solid angle $\sin\theta'_\infty > \sin\theta_\infty$ at S_∞,

$$\dot{M}(r) = \dot{M}_{>l} = \dot{M}_{\rm tot}\cos\theta_\infty(l). \quad (15)$$

In the case of solid body rotation at S_∞ (eq. [14]), we have the relation $\sin\theta_\infty = l/l_0$, and hence

$$\dot{M}(r) = \dot{M}_{\rm tot}\cos\theta_\infty(l) = \dot{M}_{\rm tot}\sqrt{1-\left(\frac{l}{l_0}\right)^2}. \quad (16)$$

Here l is a function of r, see equation (8). With the approximate relation $l^2 \approx GMr$, we get

$$\dot{M}(r) \approx \dot{M}_{\rm tot}\sqrt{1-\frac{r}{r_0}}. \quad (17)$$

3.2 Angular momentum

In the stationary inviscid problem, the specific angular momentum of the disc at a radius r, $j(r)$, equals the average angular momentum, $\bar{l}'_z$, of matter absorbed by the disc at $r' > r$. (It follows from the conservation of the accreting mass and conservation of the total accreted angular momentum.) We have,

$$j(r) = \frac{-1}{\dot{M}(r)}\int_r^{r_0} l'_z(r')\frac{\mathrm{d}\dot{M}}{\mathrm{d}r'}\mathrm{d}r' = \frac{-1}{\dot{M}_{>l}}\int_l^{l_0} l'_z\frac{\mathrm{d}\dot{M}}{\mathrm{d}l'}\mathrm{d}l'. \quad (18)$$

Here, $l'_z = l'\sin\theta'_\infty$ and $\dot{M}_{>l}$ is given by equation (15).

In the case of solid body rotation at S_∞, we have $\sin\theta_\infty = l/l_0$, $l_z = l^2/l_0$ and $\mathrm{d}\dot{M}/\mathrm{d}l = -\dot{M}_{\rm tot}(l/l_0)(l_0^2-l^2)^{-1/2}$. Working out the integral (18) then yields

$$j(r) = \frac{2}{3}l_0 + \frac{1}{3}l_z(r) = \frac{2}{3}l_0 + \frac{l^2(r)}{3l_0}, \quad (19)$$

With the approximate relation $l^2 \approx GMr$, we get

$$j(r) \approx l_0\left(\frac{2}{3} + \frac{r}{3r_0}\right). \quad (20)$$

3.3 The radial equation

The matter in the disc is not in free fall because it absorbs the infalling matter. Along with the mass of the infall, the disc also absorbs momentum that has $r-$ and $\varphi-$components ($\theta-$components

cancel for the symmetric streams from above and below). As a result, the disc receives additional acceleration in the $r-$ and $\varphi-$directions. The resulting azimuthal velocity in the disc is determined by its angular momentum, $j(r)$, which has been found from the corresponding conservation law in Section 3.2. To find the radial velocity, one needs to write down the general conservation law in differential form, $\nabla_i T^i_k = 0$, and take the $r-$component of this equation. Here T^i_k is the stress-energy tensor of the accreting gas and ∇_i is the covariant derivative in Schwarzschild space-time.

The disc internal energy and pressure are small (heat is radiated away) and we neglect their contribution to T^i_k. We also neglect viscous stresses. The stress-energy tensor then takes the simple form $T^i_k = \rho_d c^2 u^i u_k$ (see, e.g., Misner et al. 1973), where ρ_d is the disc density and $u^i = \mathrm{d}x^i/\mathrm{d}\lambda$ is the disc four-velocity. Here, λ is proper time and x^i are Schwarzschild coordinates. For the flow in the thin disc we have $u^\theta = 0$, so that $u^i = (u^t, u^r, 0, u^\varphi)$. The non-zero components of Schwarzschild metric in the equatorial plane are $g_{tt} = -(1 - r_g/r)c^2$, $g_{rr} = r/(r - r_g)$, and $g_{\theta\theta} = g_{\varphi\varphi} = r^2$.

Assuming a steady state, we derive from the $r-$component of the equation $\nabla_i T^i_k = 0$,

$$\frac{\mathrm{d}u^r}{\mathrm{d}r} = \frac{\mathrm{d}\dot{M}}{\mathrm{d}r}\frac{(\hat{u}^r - u^r)}{\dot{M}(r)} - \frac{r_g c^2}{2r^2 u^r}\left(1 - \frac{j^2}{j^2_{\rm K}}\right). \qquad (21)$$

Here, $j = u_\varphi = g_{\varphi\varphi}u^\varphi$ is the disc angular momentum calculated in Section 3.2, and

$$j^2_{\rm K} \equiv \frac{r^2 r_g c^2}{2r - 3r_g} \qquad (22)$$

is a formal notation. At $r > (3/2)r_g$, $j^2_{\rm K}$ has the meaning of the squared angular momentum for circular Keplerian rotation. At $r < (3/2)r_g$, such motion is not possible in Schwarzschild geometry, which is reflected by the fact that $j^2_{\rm K} < 0$. This is in contrast to the corresponding Newtonian problem (see Section 4) where $j^2_{\rm K} = GMr > 0$ for any r.

The $\hat{u}^r$ in equation (21) is the $r-$component of the four-velocity of matter impinging the disc at radius r,

$$\hat{u}^r = -\sqrt{\frac{r_g c^2}{r} - \frac{l^2}{r^2}\left(1 - \frac{r_g}{r}\right)}, \qquad (23)$$

with l being related to r via equation (8). In the Newtonian approximation, the factor $(1 - r_g/r)$ disappears.

Note that equation (21) is formally identical to the corresponding equation in Newtonian gravity (considering u^r as a normal Newtonian radial velocity). The relativistic effects come into the problem through $j^2_{\rm K}$, $\hat{u}^r$, and the relation (8) between l and r.

To test the radial equation, assume for a moment that inside a radius r_1 the disc does not absorb any matter. Then at $r < r_1$ we have $\dot{M}(r) = \dot{M}(r_1) = const$ and $j(r) = j(r_1) = const$, i.e., the disc matter is freely falling from r_1 with constant angular momentum. In this case, equation (21) can be rewritten as

$$\frac{\mathrm{d}}{\mathrm{d}r}\left[(u^r)^2 + \left(c^2 + \frac{j^2}{r^2}\right)\left(1 - \frac{r_g}{r}\right)\right] = 0.$$

This equation should be compared with the relation $u_i u^i = -c^2$ that holds for any time-like world-line. In particular, the relation yields the orbital energy,

$$E^2(r) = u_t^2 = -g_{tt}c^2\left[g_{rr}(u^r)^2 + \frac{u_\varphi^2}{g_{\varphi\varphi}}\right]$$

$$= c^2(u^r)^2 + c^2\left(c^2 + \frac{j^2}{r^2}\right)\left(1 - \frac{r_g}{r}\right). \qquad (24)$$

The radial equation (21) thus reproduces the correct equation $\mathrm{d}E/\mathrm{d}r = 0$ in the limit $\mathrm{d}\dot{M}/\mathrm{d}r \to 0$. The presence of $\mathrm{d}\dot{M}/\mathrm{d}r \neq 0$ and $\hat{u}_r \neq u_r$ leads to an additional acceleration term in the radial equation.

It is instructive to compare our problem with the classical Bondi-Hoyle-Lyttleton (BHL) problem (see Bondi & Hoyle 1944). In their case, accretion proceeds along a one-dimensional (1D) caustic, called accretion line. The accretion line is fed at each point by matter from an initially *plane-parallel* flow which is axisymmetric and has *zero* net angular momentum. In our case, we have a 2D accretion disc (the collision plate) which is fed by an asymptotically *isotropic* inflow with a *non-zero* net angular momentum. In contrast to the BHL accretion line, the radial momentum of matter impinging the disc is directed towards the accretor rather than outwards. As a result, we do not have the degenerate stagnation radius that exists in the BHL problem and leads to infinite number of possible solutions (cf. Bondi & Hoyle 1944).

Our radial equation (21) is similar to the BHL equation describing gas motion along the accretion line (see eq. [8] in Bondi & Hoyle 1944). The only difference is that we have an additional term proportional to $j^2/j^2_{\rm K}$. This term reflects the fact that the disc matter is rotating and a repulsive centrifugal force appears. This force will stop accretion if the angular momentum exceeds some $l_{\rm cr}$ (see Section 3.4). A stationary inviscid disc can form only in accretion flows with angular momenta below $l_{\rm cr}$.

The differential equation (21), like the BHL equation, does not admit analytical solution. We solve numerically equation (21) combined with the formulae (15), (18), (22), (23) for $\dot{M}$, j, $j^2_{\rm K}$, $\hat{u}^r$, respectively, and take into account the relation (8) between l and r. The outer boundary condition is $u^r(r_0) = \hat{u}^r$.

The solution $u^r(r)$ together with the expressions for the disc angular momentum (18) and the accretion rate (15) yield a closed description of the fast inviscid disc. The model is fully determined by the angular momentum specified at S_∞, $l(\theta_\infty)$.

3.4 The critical angular momentum

We now illustrate with the case of solid body rotation at S_∞, $l = l_0 \sin\theta_\infty$. Then l_0 is the only parameter of the problem, and the disc accretion rate, $\dot{M}(r)$, and its angular momentum, $j(r)$, are given by equations (16) and (19), respectively.

Fig. 3 shows numerical solutions for the radial velocity for three values of $l_0 \leq l_{\rm cr}$. At $l_0 = l_{\rm cr} \approx 2.62 r_g c$, the velocity profile touches zero: accretion is stopped by the centrifugal barrier. This barrier is conveniently described in terms of the effective potential, V, for radial motion (see Misner et al. 1973, p. 636, for detailed discussion). Equation (24) can be written in the form,

$$(u^r)^2 = \frac{E^2(r) - V^2(r)}{c^2}, \qquad \frac{V^2(r)}{c^2} = \left(c^2 + \frac{j^2}{r^2}\right)\left(1 - \frac{r_g}{r}\right).$$

The potential has a pit at small r, $V \to 0$ at $r \to r_g$, which describes the ability of a BH to capture surrounding matter. A body falling freely with angular momentum j will be absorbed by the BH if its orbital energy is sufficient to overcome the potential barrier enclosing the pit for high j. In the accretion disc, both the orbital energy and the angular momentum of the accreting gas change with radius. However, the same condition applies: the gas falls into the BH if $E(r)$ exceeds $V(r)$ at any r. This condition is satisfied

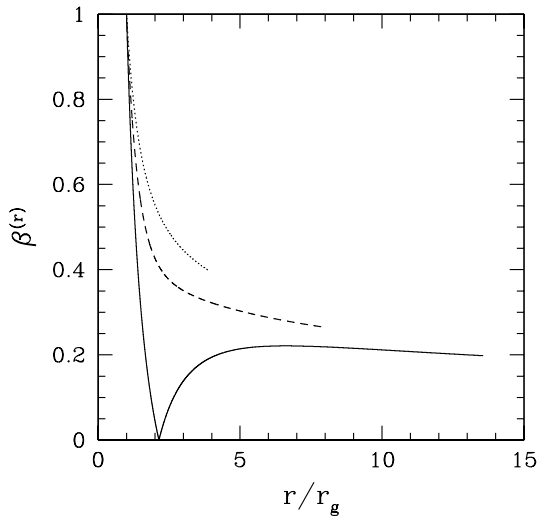

Figure 3. The radial velocity of the disc as measured by the local stationary observer, $\beta^{(r)} = (-g_{rr}/g_{tt})^{1/2}(\mathrm{d}r/\mathrm{d}t) = u^r c/E$. The dotted, dashed, and solid curves correspond to the cases $l_0 = \sqrt{2}r_g c$, $l_0 = 2r_g c$, and $l_0 = l_{\rm cr} \approx 2.62 r_g c$, respectively, (see eq. [14] for the definition of l_0). The outer radius of the disc is $r_0 \approx 2l_0^2/r_g c^2$. The disc disappears when $l_0 < l_* = 0.754 r_g c$.

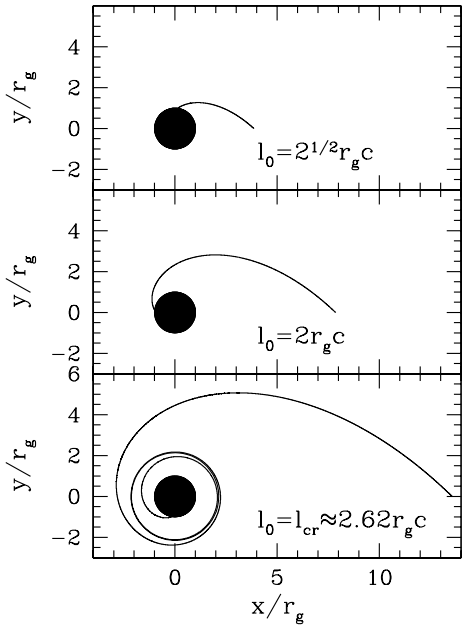

Figure 4. The trajectory of a marked point on the disc, from the outer edge into the black hole. In the critical case (bottom panel) the trajectory makes infinite number of laps at the critical radius $r_{\rm cr} \approx 2.14 r_g$ before falling into the black hole.

if $l_0 < l_{\rm cr}$. When $l_0 = l_{\rm cr}$, the curves $E(r)$ and $V(r)$ touch at $r_{\rm cr} \approx 2.14 r_g$, close to the maximum of $V(r)$.

The $\varphi-$motion of the disc can be calculated by integrating the equation $\mathrm{d}\varphi/\mathrm{d}r = u^\varphi/u^r = j/r^2 u^r$. In Fig. 4 we show the trajectory of one marked point of the disc, which moves from the outer boundary r_0 into the BH. In the critical case, $l_0 = l_{\rm cr}$, the gas makes infinite number of laps at $r_{\rm cr}$ before it falls into the BH. Note that the disc surface density, Σ, increases infinitely at $r \to r_{\rm cr}$: $\Sigma(r) = \dot{M}(r)/2\pi r u^r \to \infty$.

The maximum radius of a steady fast disc is reached in the critical case, $l_0 = l_{\rm cr}$. It equals $r_{\max} \approx 13.6 r_g \approx 27GM/c^2$. At $l_0 > l_{\rm cr}$, there is no stationary solution to the inviscid problem. This case is rather complicated, showing unstable time-dependent behaviour, and it will be studied in a separate paper (Beloborodov & Illarionov 2000). Here, we restrict our consideration to the subcritical case, $l_0 \le l_{\rm cr}$.

3.5 The energy release

The material absorbed by the fast disc at $r' > r$ and accreted down to r has changed its orbital energy from the initial parabolic value, c^2, to $E(r)$ given by equation (24). The energy released outside r thus equals

$$L_0^{>r} = \dot{M}(r)\left[c^2 - E(r)\right].$$

The total energy released by the disc is

$$L_0 = \dot{M}_d\left[c^2 - E(r_g)\right]. \qquad (25)$$

Here $\dot{M}_d = \dot{M}(r_g)$ is the total accretion rate through the disc and $c^2 - E(r_g)$ is the binding energy of gas swallowed by the black hole.

The energy liberated per unit radius,

$$\frac{\mathrm{d}L_0}{\mathrm{d}r} = \frac{\mathrm{d}}{\mathrm{d}r}\left[\dot{M}(r)\left(c^2 - E(r)\right)\right], \qquad (26)$$

can be represented as a sum of two terms, $[c^2 - E(r)]\mathrm{d}\dot{M}/\mathrm{d}r - \dot{M}(r)\mathrm{d}E/\mathrm{d}r$, both describing the inelastic collision of the infalling matter with the disc. The first term results from the difference between the orbital energies of the infalling matter before and after the collision, $\Delta E = c^2 - E(r)$. The second term is associated with the change in the orbital energy of the disc absorbing the infall, $\mathrm{d}E/\mathrm{d}r$.

In Fig. 5 we show the distribution of the liberated energy over radius, $r\mathrm{d}L_0/\mathrm{d}r$. Interestingly, the energy release peaks at $\approx 2r_g$. The sharp peak in the critical case is just at $r = r_{\rm cr}$. The peak is caused by the minimum of u^r (see Fig. 3). Here, the relative velocity between the disc and the infall increases and the inelastic collision liberates more energy. Note that in the relativistic standard disc model (Novikov & Thorne 1973) $r\mathrm{d}L/\mathrm{d}r$ peaks at $\approx 9r_g$.

3.6 The luminosity capture by the black hole

That the energy release peaks so close to the BH implies that a substantial fraction of the released luminosity, L_0, is absorbed by the black hole. We now evaluate the absorbed luminosity, $L_{\rm abs}$. The rest of disc luminosity, $L = L_0 - L_{\rm abs}$, escapes to infinity.

Assume that each element of the disc, $\mathrm{d}S$, emits radiation isotropically in its comoving frame. Let L_c be the luminosity of $\mathrm{d}S$ measured in the comoving frame, $L_{\rm loc}$ – the luminosity of $\mathrm{d}S$ measured by the local stationary observer (LSO), $\boldsymbol{\beta}$ – the local disc velocity measured by LSO (in units of c), and $\gamma = (1-\beta^2)^{-1/2}$.

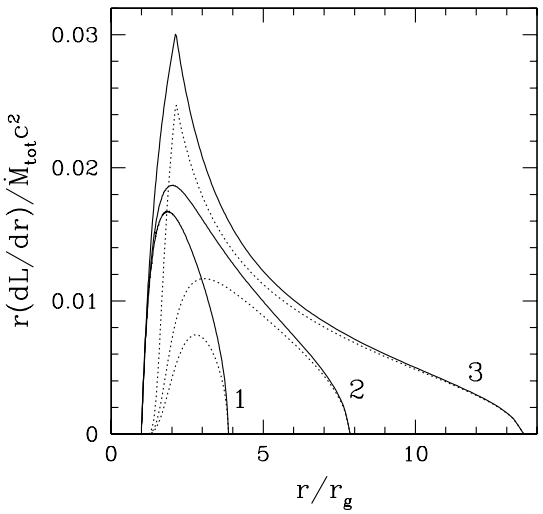

Figure 5. The radial distribution of the disc luminosity: solid curves – the released luminosity (eq. [26]), dashed curves – the observed luminosity corrected for the gravitational capture by the black hole (eqs. [28,29]). Marks 1, 2, and 3 correspond to the cases $l_0 = \sqrt{2} r_g c$, $l_0 = 2 r_g c$, and $l_0 = l_{\rm cr} \approx 2.62 r_g c$, respectively.

We then have the relation (see, e.g., Rybicki & Lightman 1979, chapter 4.8),

$$\frac{{\rm d}L_{\rm loc}}{{\rm d}\Omega} = \frac{L_c}{4\pi\gamma^4(1-\boldsymbol{\beta}\cdot\boldsymbol{\Omega})^3}, \qquad (27)$$

where $\boldsymbol{\Omega}$ is a unit vector specifying direction of an emitted photon in the LSO frame, ${\rm d}\Omega$ is the element of the solid angle. Relation (27) takes into account that the accretion disc is steady, so that the luminosity produced by each ${\rm d}S$ is constant and the velocity field on the disc is constant. Then there is no retardation effect (cf. Rybicki & Lightman 1979, p. 141). The local luminosity emitted in 4π, as measured by LSO, is equal to the rest frame luminosity, $L_{\rm loc} = L_c$.

Consider the local tetrade $(e^i_{(t)}, e^i_{(r)}, e^i_{(\theta)}, e^i_{(\varphi)})$ and let $(\beta^{(r)}, 0, \beta^{(\varphi)})$ and $(\Omega^{(r)}, \Omega^{(\theta)}, \Omega^{(\varphi)})$ be the tetrade components of $\boldsymbol{\beta}$ and $\boldsymbol{\Omega}$, respectively. β^α ($\alpha = 1, 2, 3$) is related to the four-velocity of the disc, u^i, by $\beta^{(\alpha)} = (u^\alpha/u^t)(-g_{\alpha\alpha}/g_{tt})^{1/2}$, and $\gamma = u^t(-g_{tt})^{1/2}$. $\Omega^{(\alpha)}$ can be written as $\Omega^{(r)} = -\cos\hat\theta$, $\Omega^{(\theta)} = -\sin\hat\theta\sin\hat\varphi$, $\Omega^{(\varphi)} = \sin\hat\theta\cos\hat\varphi$, and ${\rm d}\Omega = \sin\hat\theta {\rm d}\hat\theta {\rm d}\hat\varphi$. Equation (27) now takes the form

$$\frac{{\rm d}L_{\rm loc}}{{\rm d}\hat\theta {\rm d}\hat\varphi} = \frac{L_{\rm loc}\sin\hat\theta}{4\pi\gamma^4[1+\beta^{(r)}\cos\hat\theta - \beta^{(\varphi)}\sin\hat\theta\cos\hat\varphi]^3}.$$

The black hole absorbs radiation emitted within a cone $\hat\theta < \hat\theta_{\rm abs}(r)$ (see Misner et al. 1973, p. 675), where

$$\sin^2\hat\theta_{\rm abs} = \frac{27 r_g^2}{4r^2}\left(1 - \frac{r_g}{r}\right).$$

$\hat\theta_{\rm abs} < \pi/2$ at $r > (3/2)r_g$ and $\hat\theta_{\rm abs} > \pi/2$ at $r < (3/2)r_g$. At $r = r_g$, $\hat\theta_{\rm abs} = \pi$, i.e., all the radiation is absorbed.

The captured fraction of radiation emitted at a radius r is

$$\kappa(r) = \int_0^{2\pi}\int_0^{\hat\theta_{\rm abs}} \frac{\sin\hat\theta\,{\rm d}\hat\theta\,{\rm d}\hat\varphi}{4\pi\gamma^4[1+\beta^{(r)}\cos\hat\theta - \beta^{(\varphi)}\sin\hat\theta\cos\hat\varphi]^3}. \qquad (28)$$

The released and captured power from ${\rm d}S$ as measured at infinity is $L_{\rm loc}(-g_{tt})$ and $\kappa L_{\rm loc}(-g_{tt})$, respectively. The resulting radial distribution of the observed luminosity is

$$\frac{{\rm d}L}{{\rm d}r} = \frac{{\rm d}L_0}{{\rm d}r}\left[1 - \kappa(r)\right]. \qquad (29)$$

Equation (29) is exact for an optically thin disc only. An optically thick disc partly intercepts its own radiation owing to the gravitational bending of light near the black hole, and reemits this radiation. As a result of this self-illumination, the radial distribution of the disc luminosity changes. We here neglect these effects and use equations (28,29) to estimate the captured luminosity.

The result is shown in Fig. 5 by the dotted curves. The capture of radiation by the BH markedly reduces the observed luminosity of the disc, especially when l_0 is small. Then the radial velocity is large (see Fig. 3) and the capture is enhanced by the Doppler beaming of the disc radiation into the black hole. In the critical case, $l_0 = l_{\rm cr}$, the inflow is decelerated at $r \approx 2r_g$, and the luminosity capture is less efficient.

3.7 The radiative efficiency

There are a few ways to define the efficiency: (i) $\eta = L_0/\dot M_{\rm tot}c^2$, (ii) $\eta = L/\dot M_{\rm tot}c^2$, (iii) $\eta = L_0/\dot M_d c^2$, and (iv) $\eta = L/\dot M_d c^2$. We choose the first definition as a basic one and compute the other three for comparison. The results are shown in Fig. 6.

The maximum efficiency, $\eta \approx 0.0372$, is achieved in the critical case, $l_0 = l_{\rm cr}$. It is smaller than the efficiency of the standard disc around a Schwarzschild black hole, $\eta = 1 - 2\sqrt{2}/3 \approx 0.0572$, however it is comparable to this value. We conclude that the fast inviscid disc is quite an efficient regime of accretion.

4 NEWTONIAN FAST DISC

The Newtonian approximation cannot give adequate description of the fast disc around a black hole. However, in the case of accretion onto a non-relativistic star of mass M and radius $R_* \gg 2GM/c^2$, a similar problem can be formulated in Newtonian gravity. The importance of the relativistic effects is well seen when comparing the fast disc in Schwarzschild geometry with its Newtonian counterpart.

4.1 The disc equations

The Newtonian disc fed by matter coming from S_∞ with angular momentum $l(\theta_\infty)$ is described by the same equations as the relativistic disc except for a few changes which we point out below. In particular, all the formulae for the disc accretion rate, $\dot M(r)$, (Section 3.1) and its angular momentum, $j(r)$, (Section 3.2) apply to the Newtonian case. The only difference is that the relation

$$r = \frac{l^2}{GM} \qquad (30)$$

between a streamline angular momentum and its collision radius should now be used instead of equation (8). It implies that the condition for the disc formation ($r > R_*$) now reads $l > l_* =$

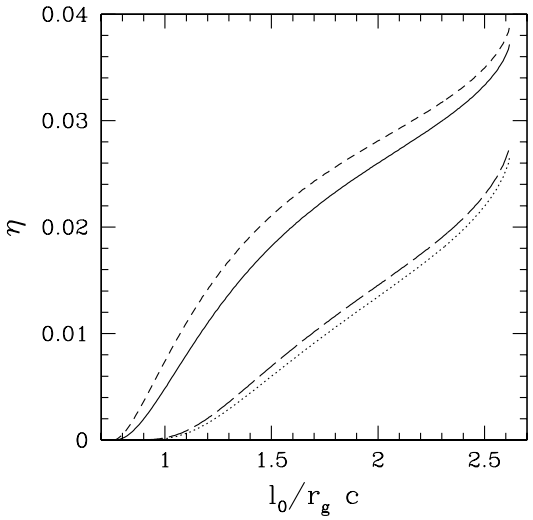

Figure 6. The efficiency of accretion, η, versus l_0. The four curves correspond to different definitions of efficiency: solid curve – $\eta = L_0/\dot{M}_{\rm tot}c^2$, dashed curve – $\eta = L_0/\dot{M}_d c^2 = 1 - E(r_g)/c^2$, dotted curve – $\eta = L/\dot{M}_{\rm tot}c^2$, long dashed curve – $\eta = L/\dot{M}_d c^2$. Here, L_0 is the power released by the disc (see eq. [25]), L is the luminosity corrected for the capture by the black hole (see Section 3.6), $\dot{M}_{\rm tot}$ is the total accretion rate (including the polar part that plunges into the event horizon before crossing the equatorial plane), and $\dot{M}_d$ is the accretion rate through the disc.

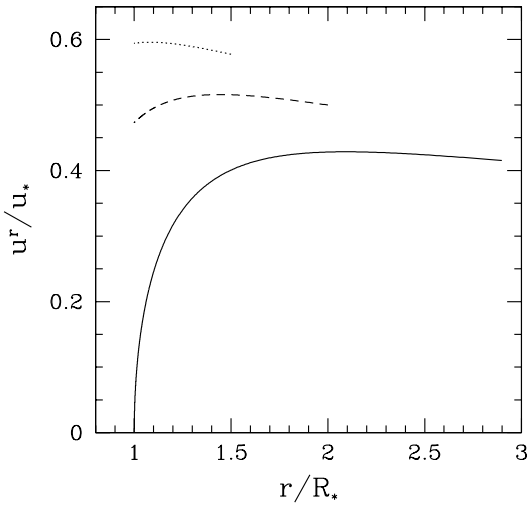

Figure 7. The radial velocity of the Newtonian fast disc, $u^r(r) = {\rm d}r/{\rm d}t$. The dotted, dashed, and solid curves show the cases $l_0 = (\sqrt{3}/2)R_*u_*$, $l_0 = R_*u_*$, and $l_0 = l_{\rm cr} \approx 1.204R_*u_*$, respectively (see eq. [14] for the definition of l_0). Here, $u_* \equiv (2GM/R_*)^{1/2}$. The outer radius of the disc is $r_0 = 2l_0^2/R_*u_*^2$. The disc disappears when $l_0 < l_* = R_*u_*/\sqrt{2}$.

$(GMR_*)^{1/2}$. In fact, one can use equation (30) as a good approximation even in Schwarzschild geometry (see Fig. 2), so this is a minor change.

The important difference between the Newtonian and relativistic cases appears only in radial motion described by equation (21). Although the radial equation is formally identical in both cases, the expression for $j_{\rm K}^2$ appearing in this equation is crucially different. In Newtonian case,

$$j_{\rm K}^2 = GMr. \tag{31}$$

The different expressions (22) and (31) for $j_{\rm K}^2$ result in different effective potentials for radial motion (see Section 4.2).

The value of $\hat{u}^r$ (the radial velocity of matter impinging the disc) in the Newtonian case is (compare with eq. [23]),

$$\hat{u}^r = -\sqrt{\frac{GM}{r}}. \tag{32}$$

The equations for $r(l)$, $j_{\rm K}^2(r)$, and $\hat{u}^r$ are the only equations changed as compared to the BH case. The major change is equation (31) that makes the Newtonian fast disc crucially different from its relativistic counterpart (see below).

We now assume the same inflow at S_∞ as in the relativistic problem, ${\rm d}\dot{M}/{\rm d}\Omega_\infty = \dot{M}_{\rm tot}/4\pi$ and $l(\theta_\infty) = l_0 \sin\theta_\infty$, and compute the structure of the Newtonian fast disc. We solve numerically equation (21) coupled with algebraic expressions (16), (19), (30), (31), and (32) for $\dot{M}(l)$, $j(l)$, $r(l)$, $j_{\rm K}(r)$, and $\hat{u}^r(r)$, respectively. The outer radius of the disc is given by $r_0 = l_0^2/GM$, and the outer boundary condition is $u^r(r_0) = \hat{u}^r(r_0)$. At the inner boundary, $r = R_*$, the accreting matter is absorbed by the central object.

The natural units of length and velocity in the problem are the radius of the accretor, R_*, and the free-fall velocity on its surface, $u_* = (2GM/R_*)^{1/2}$. Correspondingly, the angular momentum will be measured in units of R_*u_*.

4.2 The critical angular momentum

Like the BH case, there exists a critical angular momentum, $l_{\rm cr}$, such that accretion flows with $l > l_{\rm cr}$ are stopped by the centrifugal barrier. The effective potential for radial motion in the disc is

$$V(r) = -\frac{GM}{r} + \frac{j^2}{2r^2}.$$

The important difference from the BH case is that the pit at small r is now absent, $V(r) \to \infty$ at $r \to 0$, and the potential produces a stronger repulsive centrifugal force. It leads to tighter constraints on the angular momentum of the fast disc regime. Numerically, we find $l_{\rm cr} = 1.204R_*u_*$. The minimum angular momentum necessary for the disc formation is $l_* = R_*u_*/\sqrt{2} \approx 0.707R_*u_*$. The fast disc solution thus exists at $0.707 < l_0/R_*u_* < 1.204$.

At $l_0 = l_{\rm cr}$, the critical ("centrifugal reflection") point with $u^r = 0$ first appears at the inner boundary of the disc, $r = R_*$. The disc streamlines then touch the accretor with $u^r \to 0$. The gas moving from the outer edge, r_0, to the touching point rotates by angle $\Delta\varphi \approx 2.21$. The critical behaviour of the BH disc (see Fig. 4) was qualitatively different: $r_{\rm cr} \approx 2.14r_g$ was twice as large as the BH radius and gas rotated infinite number of laps.

The maximum radius of the fast disc is achieved in the critical case, $r_{\max}/R_* = l_{\rm cr}^2/GMR_* \approx 2.90$. It should be compared with $r_{\max}/r_g \approx 13.6$ in the BH case. One concludes that the large ex-

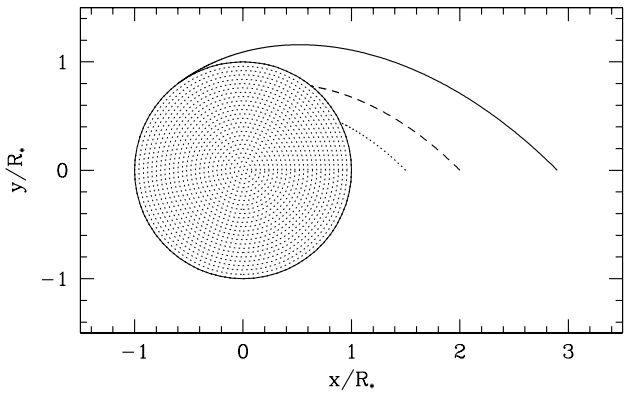

Figure 8. The trajectory of a marked point on the Newtonian fast disc, from the outer edge onto the surface of the accretor, R_*. The dotted, dashed, and solid curves show the cases $l_0 = (\sqrt{3}/2)R_*u_*$, $l_0 = R_*u_*$, and $l_0 = l_{\rm cr} \approx 1.204R_*u_*$, respectively.

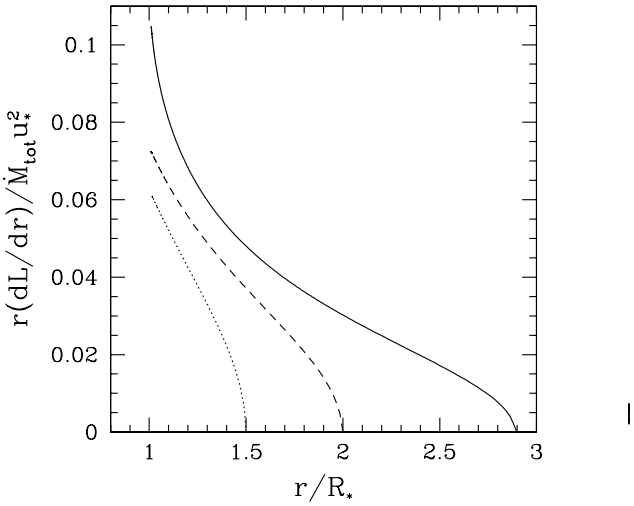

Figure 9. The radial distribution of the Newtonian fast disc luminosity in units of $\dot{M}_{\rm tot}u_*^2$. The dotted, dashed, and solid curves show the cases $l_0 = (\sqrt{3}/2)R_*u_*$, $l_0 = R_*u_*$, and $l_0 = l_{\rm cr} \approx 1.204R_*u_*$, respectively.

tension of the BH fast disc was caused by purely relativistic effects, namely, by the pit in the effective potential.

4.3 The disc luminosity

The energy released by the disc outside a given radius r equals

$$L^{>r} = -E(r)\dot{M}(r).$$

Here, $E(r)$ is the Newtonian specific orbital energy,

$$E(r) = \frac{(u^r)^2}{2} + \frac{j^2}{2r^2} - \frac{GM}{r}. \qquad (33)$$

$E = 0$ for the parabolic infall above the equatorial plane, and the binding energy of the disc matter equals $-E(r)$.

The total luminosity of the disc is given by

$$L = -E(R_*)\dot{M}_d, \qquad (34)$$

where $\dot{M}_d = \dot{M}(R_*) = \dot{M}_{\rm tot}(1 - R_*/r_0)^{1/2}$ is the accretion rate through the disc and $-E(R_*)$ is the binding energy of matter that reaches the accretor. We now do not make any distinction between the released and observed luminosities, even though a part of the disc luminosity strikes the accretor. In contrast to the BH case, this part of the luminosity is reemitted by the accretor and eventually it also contributes to the total luminosity.

The energy liberated per unit radius is

$$\frac{{\rm d}L}{{\rm d}r} = \frac{\rm d}{{\rm d}r}\left[-E(r)\dot{M}(r)\right]. \qquad (35)$$

In Fig. 9 we show the distribution of the liberated energy over radius, $r{\rm d}L/{\rm d}r$. In contrast to the BH case, the luminosity distribution peaks at $r = R_*$ (compare with Fig. 5).

Fig. 10 shows the radiative efficiency of the Newtonian fast disc as a function of l_0. The efficiency increases with increasing l_0 and reaches its maximum at $l_0 = l_{\rm cr}$. There is a simple relation between the maximum efficiciency and $l_{\rm cr}$. The efficiency is determined by the binding energy of the disc matter at $r = R_*$ (see eq. [34]). In the critical case,

$$-E(R_*) = \frac{GM}{R_*} - \frac{j^2(R_*)}{2R_*^2} = \frac{GM}{R_*}\left[1 - \frac{1}{2}\left(\frac{2l_{\rm cr}}{3l_*} + \frac{l_*}{3l_{\rm cr}}\right)^2\right].$$

We here made use of the fact that $u^r = 0$ at $r = R_*$ and also of the formula $j(R_*) = (2/3)l_0 + l_*^2/3l_0$ (see eq. [19]). Amusingly, the critical binding energy of the Newtonian fast disc in units of u_*^2, $-E(R_*)/u_*^2 \approx 0.0572$, exactly coincides with the binding energy of the marginally stable Keplerian orbit around a Schwarzschild BH, $(c^2 - E)/c^2 = 1 - 2\sqrt{2}/3 \approx 0.0572$.

5 DISCUSSION

5.1 Special features of the fast disc regime

There are two principle features of the accretion regime studied in this paper, which make it different from previous models of rotating accretion flows onto black holes:

(i) The Compton cooled quasi-spherical inflow is super-sonic (freely falling) until it reaches the caustic (the collision plate). The radiative shocks associated with collision are held-down to the caustic. This regime takes place at sufficiently high accretion rates (see Section 2.3). A similar behaviour (held-down shock at high $\dot{M}$) was found for spherical accretion onto a neutron star (see Shapiro & Salpeter 1975).

(ii) The accretion disc formed in the collision plate has sub-Keplerian angular momentum and high radial velocity. In addition, the disc matter is pushed towards the BH by the infalling flow. As a result, the disc can overcome the centrifugal barrier and accrete fast in a stationary regime without any horizontal viscous

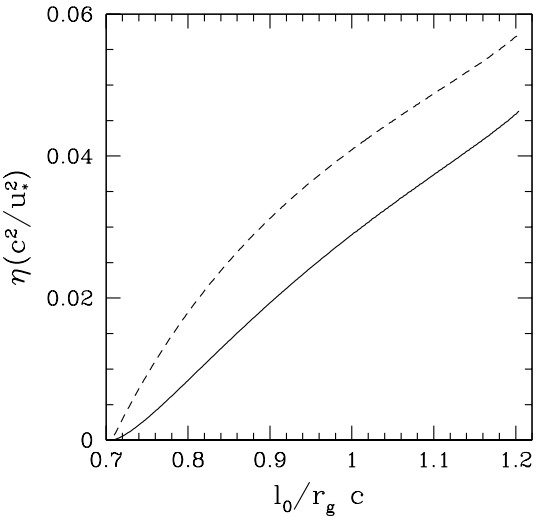

Figure 10. The efficiency of the Newtonian fast disc, η, in units of u_*^2/c^2. The two curves correspond to different definitions of efficiency: solid curve – $\eta = L/\dot{M}_{\rm tot}c^2$, dashed curve – $\eta = L/\dot{M}_d c^2 = -E(R_*)/c^2$, where $M_d(l_0) = \dot{M}_{\rm tot}\sqrt{1-(l_*/l_0)^2}$ is the accretion rate through the disc.

stresses. The relativistic pit in the effective potential helps dramatically in this process and allows the fast disc radius to be as large as $\approx 13.6r_g \approx 27GM/c^2$ (see Section 3.4). By contrast, in the corresponding Newtonian problem, the maximum radius of the fast disc is $2.9R_*$ only, where R_* is the accretor radius (see Section 4.2).

The fast disc regime resembles the original (free-fall) version of Bondi-Hoyle-Lyttleton accretion, with the accretion line replaced by the collision plate (see discussion in Section 3.3).

5.2 The generated spectrum

As we argued in Section 1, small-scale discs are likely to form in wind-fed X-ray binaries and they are also possible in AGNs. We now briefly discuss the expected X-ray spectrum emitted by the fast small-scale disc. First of all note that discs with $\dot{m} > 1$ ($L > \eta L_{\rm E}$) have optical depths $\tau_{\rm T} > 1$. The disc emission then consists of two components: L_h – the hard radiation from the top optically thin layer that radiates the vertical kinetic energy of the infall, and L_s – the radiation produced inside the optically thick disc where the horizontal velocities of the infall and the disc get equalised (see Section 2.3). Since L_s comes out from the optically thick material, it is mostly soft radiation. By contrast, L_h is generated by unsaturated Comptonization in the hot layer with the electron temperature $kT_e \sim 100$ keV (see Section 2.3). The Comptonized X-rays have a standard power-law spectrum with a break at ~ 100 keV. The soft component L_s can be the main source of seed photons for Comptonization in the hot layer.

The expected two-component spectrum is reminiscent of the observed spectra in galactic black hole sources and AGNs (see Zdziarski 1999 for a review). The observed spectra are well fitted by two phenomenological models: (i) a hot accretion disc surrounded by a cold gaseous ring or (ii) a hot corona atop a cold disc. Both models are usually considered as modifications of the standard α-disc in which the energy is released as a result of viscous stresses in a flow with high angular momentum (see Beloborodov 1999 for a review). The small-scale disc studied here generates a similar spectrum and it may provide a preferable explanation of the observed spectra in some cases. In general, the power-law spectrum produced by unsaturated Comptonization is degenerate, i.e., it does not determine the plasma heating mechanism and/or the flow pattern. More detailed studies of the spectrum features such as Fe Kα line and the Compton reflection bump from the optically thick disc might help to break the degeneracy.

5.3 Issues for further study

(i) Exact calculations of the emitted X-ray spectrum require detailed modelling of radiative transfer in the post-shock plasma. The slope of the spectrum is controlled by the Compton amplification factor of the hot layer (see, e.g., Beloborodov 1999), which is determined by the soft luminosity entering the hot layer from below.

(ii) At high $\dot{M}$, the quasi-spherical infall gets so optically thick that it will trap the inner radiation and tend to advect it into the BH (Begelman 1978). The trapping becomes efficient when the timescale of radiative diffusion through the infall is longer than the accretion time-scale. For the typical radius, $r \sim 2r_g$, where most of the fast disc luminosity is produced, the trapping occurs at $\dot{m} \gtrsim 4$. The corresponding reduction of the observed luminosity and the impact on the X-ray spectrum should be taken into account.

(iii) Throughout the paper, we assumed that the BH has a small spin. A similar problem can be solved for a rotating black hole.

(iv) We did not consider here the case $l > l_{\rm cr}$ where accretion is stopped by the centrifugal barrier. At high l, the fast disc should transform into the standard accretion disc. This transition will be studied elsewhere (Beloborodov & Illarionov 2000).

Acknowledgments

We thank J. Poutanen for comments on the manuscript. This work was supported by the Swedish Natural Science Research Council, the Wenner-Gren Foundation for Scientific Research, and RFBR grant 00-02-16135.

REFERENCES

Begelman M. C., 1978, MNRAS, 184, 53
Beloborodov A. M., 1999, in Poutanen J., Svensson R., eds, High Energy Processes in Accreting Black Holes. ASP Conf. Series, 161, p. 295
Beloborodov A. M., Illarionov A. F., 2000, in preparation
Bisnovatyi-Kogan G. S., Ruzmaikin A. A., 1974, Ap&SS, 28, 45
Bondi H., Hoyle F., 1944, MNRAS, 104, 273
Draine B. T., McKee C. F., 1993, ARA&A, 31, 373
Frank J., King A., Raine D., 1985, Accretion Power in Astrophysics, Cambridge Univ. Press, Cambridge
Hills J. G., 1975, Nature, 254, 295
Igumenshchev I. V., Illarionov A. F., Abramowicz M. A., 1999, ApJ, 517, L55
Illarionov A. F., Beloborodov A. M. 2000, MNRAS, submitted
Illarionov A. F., Kompaneets D. A., 1990, MNRAS, 247, 219
Illarionov A. F., Sunyaev R. A., 1975, A&A, 39, 185
Mészáros P., 1975, A&A, 44, 59
Misner C.W., Thorne K.S., Wheeler J.A., 1979, Gravitation. Freeman, San Francisco

Novikov I. D., Frolov V. P., 1989, Physics of Black Holes. Kluwer, Dordrecht, p. 33
Novikov, I.D., Thorne, K.S. 1973, in de Witt C., de Witt B.S., eds, Black Holes. Gordon & Breach, New York, p. 343
Pringle J. E., 1981, ARA& A, 19, 137
Rybicki G.B., Lightman A.P., 1979, Radiative Processes in Astrophysics. Wiley, New York
Shapiro S. L., 1973, ApJ, 180, 531
Shapiro S. L., Lightman A. P., 1976, ApJ, 204, 555
Shapiro S. L., Salpeter E. E., 1975, ApJ, 198, 671
Spitzer L. Jr., 1962, Physics of Fully Ionized Gases. Interscience, New York
Shvartsman V. F., 1971, Soviet Astr., 15, 377
Tanaka Y., Lewin W. H. G., 1995, in Lewin W. H. G., van Paradijs J., van den Heuvel E. P. J., eds, X-ray binaries. Cambridge Univ. Press, Cambridge, p. 126
Zdziarski A. A., 1999, in Poutanen J., Svensson R., eds, High Energy Processes in Accreting Black Holes. ASP Conf. Series, 161, p. 16
Zel'dovich Ya. B., Shakura N. I., 1969, Soviet. Astron., 13, 175